جامعة عين شمس

Faculty of Women for, Arts, Science, and Education

Scientific Publishing Unit

Journal of Scientific Research in Science

Basic Sciences

Volume 38, Issue 1, 2021

ISSN 2356-8372 (Online) \ ISSN 2356-8364 (print)

Journal of Scientific Research in Science 2021, 38, (1): 36-57

Contents lists available at EKB

Journal of Scientific Research in Science

Journal homepage: https://jsrs.journals.ekb.eg/

Characterization of structural, electrical conductivity and dielectric properties of 1',3'-dihydro-1',3',3'-trimethyl-6-nitrospiro[2H-1benzopyran-2,2'[2H] indole] compound

E.E. Elgarhy [1,*], M.M. El-Nahass [2], H.A. Zayed [1], H. A. M. Ali[2]

[1] Physics Department, Faculty of Woman for Art, Sciences and Education, Ain Shams University, Cairo, Egypt.

[2] Physics Department, Faculty of Education, Ain Shams University, Rorxy Square, 11757, Cairo, Egypt.

Abstract

The structural properties of 1',3'-dihydro-1',3',3'-trimethyl-6-nitrospiro [2H-1-benzopyran-2,2'-[2H]indole] (DTNBI) characterized using X-ray diffraction. DTNBI's powder has a monoclinic polycrystalline structure. The DTNBI's lattice constant of unit cell are (a = 29.912 Å, b = 18.815 Å, and c = 13.062 Å). The mean crystallite size and strain were evaluated using the formula of Scherrer, Williamson-Hall, and Size-Strain plots methods. In the frequency range of 40 to 5×10^6 Hz, the dependence of ac conductivity was studiedforthe bulk DTNBI upon different temperatures (303-363 K). The prevailing mechanism for the ac conduction was the correlated barrier hopping model for bulk DTNBI.The dielectric constant and the dielectric loss were also studied. The dielectric polarization mechanism of bulk DTNBI used to explain the behavior of the real, ε_1, and imaginary, ε_2, components of the complex dielectric constant. Reliance of dc and ac conductivity of bulk DTNBI follows the law of Arrhenius. The activation energy of both dc and ac conduction for bulk DTNBI were calculated and the dielectric characteristics were examined via complex electric modulus formalism.

Keywords: Structural properties; Electricalconductivity; Spiropyrans.

1- Introduction

Organic semiconductor materials get special attention, as they have optoelectronic and electrical accomplishments. They have processing properties for electronic system design and manufacturing [1]. These varied advantages are due to the variety of structures in which organic compounds can be manufactured in forms such as bulk and thin films in which electric charges transfer through these structures [2]. Organic semiconductors are technically important for electronics with convenient, innovative

***Corresponding author:** E.E.Elgarhy, Physics Department, Faculty of Women for Arts; Science and Education, Ain Shams University.

E-mail: eman.elgarhy@women.asu.edu.eg

and high-execution behavior. Organic devices make an appealing balance between efficiency and cost through simplicity and functionality achieved by molecular engineering [3-7].The optimum conditions, the analysis of electrical data and the electrical transport mechanisms of these materials are important to study the materials' electrical properties. The characterization of the device parameters should be studied by Alternating current (ac) measurements [8-13].

A class of organic photochromic compounds is spiropyrans (SP). The molecular structure of photochromic compounds will change during photochromic process, which alters the absorption spectrum of the dye [14,15]. Spiropyran as an important photochromic compound displays coloration upon UV light by cleavage of the spiro C-O bond and isomerization from a ring-closed and non-polar spiro (SP) form to a ring-opened and zwitterionic merocyanine (MC) form [16]. Recently, these compounds have a huge number of potential applications, such as variable optical transmission materials, optical delay generators, optical storage, UV sensors, dosimeter, nanomedicine application as ondemand drug delivery, and reliable sensor, due to fast response time with good photo-fatigue resistance [17,18]. One of these compounds is 1',3'-dihydro-1',3',3'-trimethyl-6-nitrospiro[2H-1-benzopyran-2,2'-[2H]indole] with the abbreviation of DTNBI. Figure 1 shows DTNBI molecular structure. There is no research on its structural and electrical properties, to our knowledge.

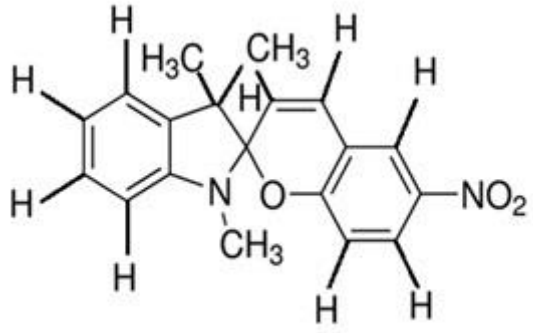

Fig .1 Molecular structure of (DTNBI).

The current work's goal is to index the structural crystallization of 1', 3'-dihydro-1',3',3'-trimethyl-6-nitrospiro [2H-1-benzopyran-2,2' [2H]indole] compound,DTNBI, estimating the crystallite size and lattice strain using different

methods. As well as the associated ac electrical conductivity together with dielectric properties of bulk DTNBI in the shape of pellets, to specify the conduction mechanism nature involved in the frequency range (40 to 5×10^6 Hz) under varying temperature in range of 303-363 K.

2- Experimental techniques:

The powder of DTNBIwas procured from Aldrich Chem. Co. and it used as received without further purification. The compound was noted as DTNBI. The XRD technique was used to explore the structural characteristics of DTNBI. The structural features of the powder were studied using a Philip X-ray diffractometer (model X' pert) with monochromatic Cuk_α radiation with wavelengths (λ= 1.542Å) working at 50 kV and 40 mA.The DTNBI powder compressed under sufficient pressure in the shape of a pellet (area of 1.33×10^{-4} m^2) and a thickness of 1.04×10^{-4} m for Ac conductivity and dielectric measurements.Using a high vacuum coating equipment (Edwards E 306A), a DTNBI pellet was sandwiched between two evaporated aluminum electrodes.

Specifically designed to reduce stray capacitance, the sample was put in a holder.The frequency range was from 40 to 5×10^6 Hz.In order to determine the sample's temperature, a calibrated Cr-Al thermocouple connected to a temperature controller (TCN4M-24R Aulonics-Korea) over a temperature range of 303-363 K was used. A programmable automatic RLC bridge, the Hioki 3532 Hitester model, was utilized to calculate certain parameters for the ac measurements which are the impedance Z, capacitance C, and loss tangent tan δ.

3- Results and discussion

3.1 Structural properties:

Figure 2 shows the DTNBI powder X-ray diffraction (XRD) pattern. Many of the diffraction peaks appeared in the powder pattern. The CHECK CELL computer software was used to estimate the indexing of the Miller indices of all peaks as well as the lattice constants for powder of DTNBI [19]. The lattice constants are a = 29.912 Å, b = 18.815 Å, and c = 13.062 Å for DTNBI which has a monoclinic structure with space group (P2). Using Scherrer's equation [20-22], the average crystallite size D,

determined by knowing the peak's width of ($\bar{5}11$) diffraction peak, which is substantially stronger in the XRD pattern of DTNBI:

$$D = \frac{k_S \lambda}{\beta \cos\theta} \quad (1)$$

Here, β is full-width at half maximum of the peak, θ is the peak position andk_s(=0.94)is a Scherrer's constant. For the diffraction peak ($\bar{5}11$), the measured D of DTNBI was 29.75 nm.

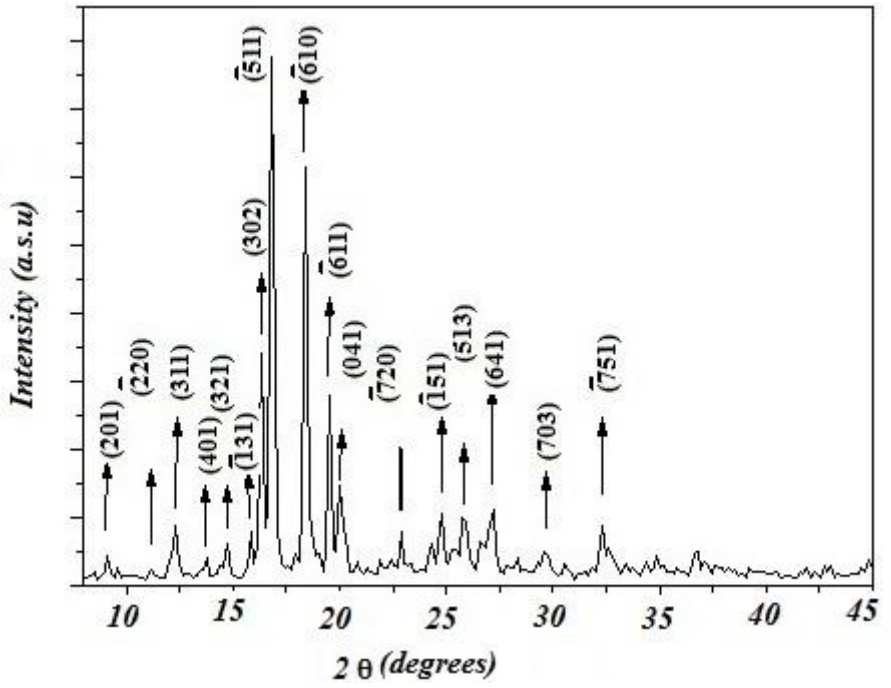

Fig.2. XRD of DTNBl in the powder form.

Besides that, the Williamson-Hall (W-H) methode will be used to calculate the crystallite's average size D, and strain ε.In the (W-H) analysis, asimplified form of integral breadth used to estimate D and ε by taking into account the width of the diffraction peak as a function of the 2θ˚ using the equation [23]:

$$\beta \cos\theta = \left(\frac{k_S \lambda}{D}\right) + (4\varepsilon \sin\theta) \quad (2)$$

The relation between (βcosθ) and (4 sinθ) is presented in Fig.3. The D and ε values of DTNBI form are evaluated from the slopes and the intercepts that obtained for the linear fit for experimental data and were given in Table 1.The line broadening was identified by the W-H plots as isotropic.An average size-strain plot (SSP) can be also used to generate a more accurate assessment of the size-strain parameters. The

'crystallite size' profile is assumed to be defined by a Lorentzian function and the 'strain profile' by a Gaussian function in this system, and assigned by [24]:

$$(d\beta\cos\theta)^2 = \left(\frac{k_s\lambda}{D}\right)(d^2\beta\cos\theta) + \left(\frac{\varepsilon}{2}\right)^2 \quad (3)$$

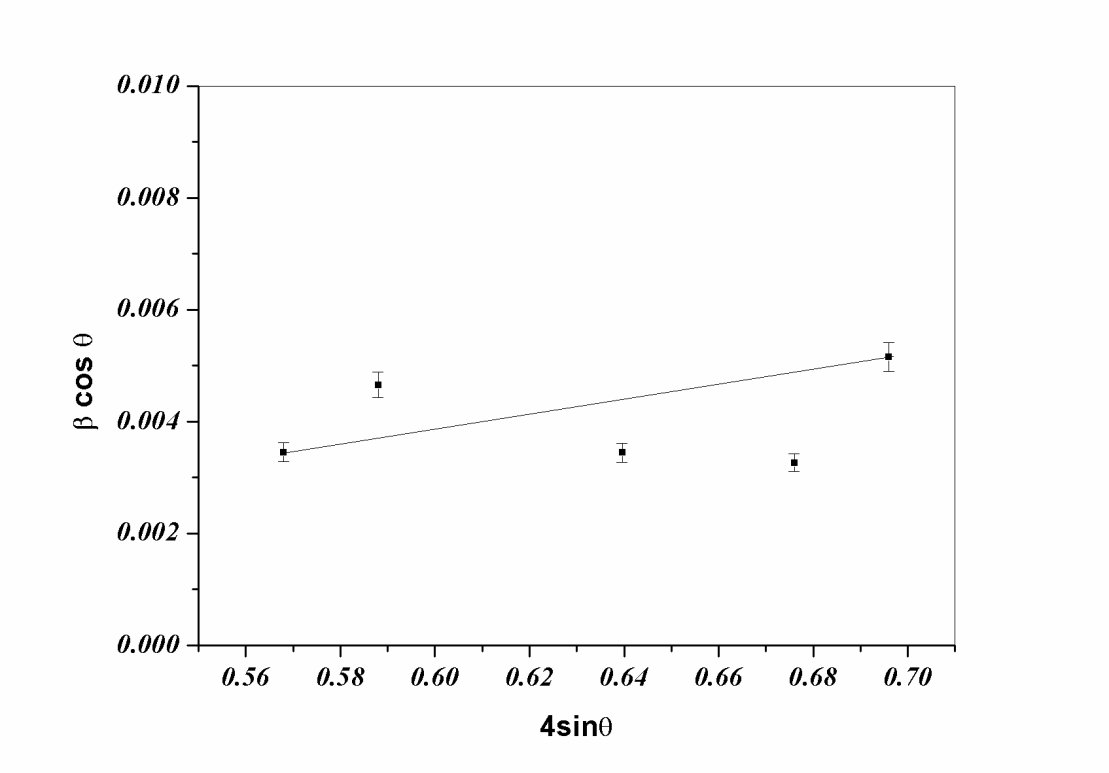

Fig 3. Plot of (βcosθ) versus and (4 sinθ).

Fig.4 shows the plot of $(d\beta\cos\theta)^2$ versus $(d^2\beta\cos\theta)$. The data is linearly fitted and the values of the crystallite size and strain of (DTNBI) are obtained and listed in Table 1. From these different methods, there are comparable vibration in average crystallite size values. Thus, the strain in various forms has effect on the average crystallite size of DTNBI nanoparticles. Using the W-H and SSP methods respectively, the strain has 1.37 $x10^{-3}$ and 2.9 $x10^{-3}$values.

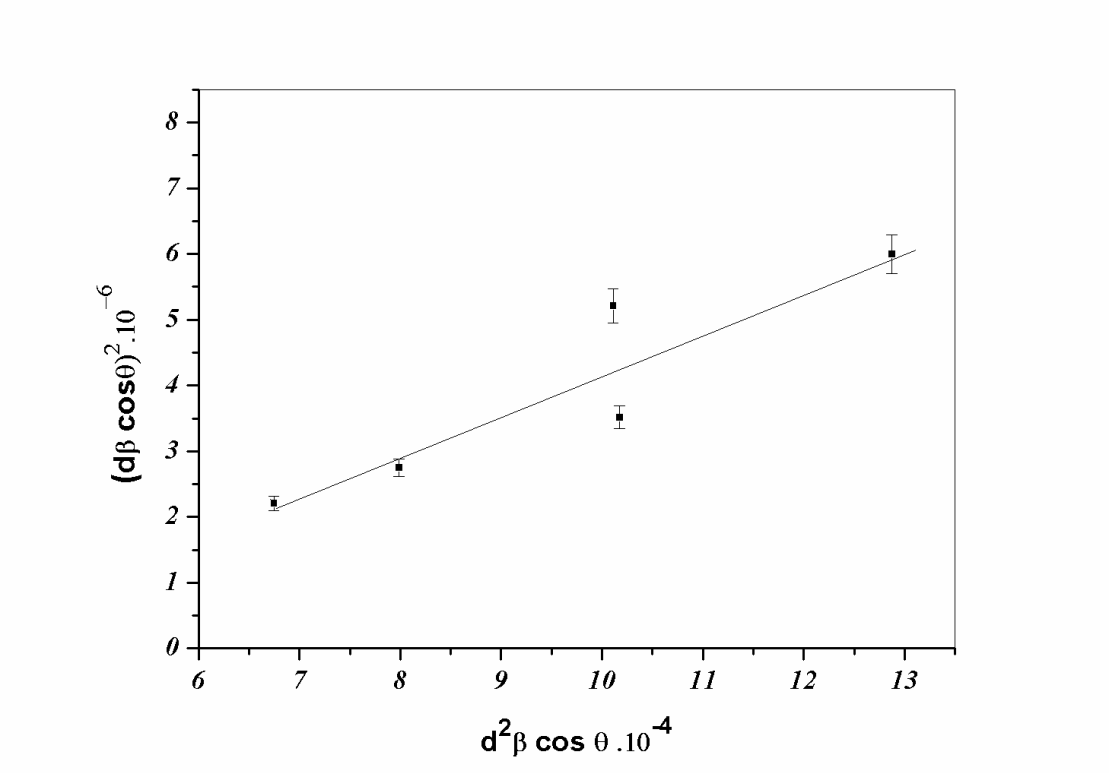

Fig 4. Plot of (d β cosθ)^2 versus (d^2 βcosθ).

Table 1: The calculated values of the mean crystallite size and strain of DTNBI.

Scherrer method	Williamson-Hall method		Size-strain plot method	
D (nm)	D (nm)	ε ×10^{-3}	D (nm)	ε ×10^{-3}
29.75	36.6	1.37	22.9	2.9

3.2 Electrical Conductivity:

The total conductivity, $\sigma_t(\omega=2\pi f)$, as a function of angular frequencyforDTNBI is illustrated in Fig.5 at various temperatures. It is evident that $\sigma_t(\omega)$ stays constant at low frequency, then it increases with increasing frequency. This behavior was pointed in several studied [21,25].The total conductivity can be represented over a broad ω and T range by the relation [26]:

$$\sigma_t(\omega, T)= \sigma_{dc}(T) + \sigma_{ac}(\omega, T) \quad (4)$$

where σ_{dc} is the dc conductivity and independent on frequency. σ_{dc} values can be acquired by extrapolating the experimental data of σ_t at low frequency till to zero value. On the other part,theσ_{ac} is the frequency dependent conductivity.

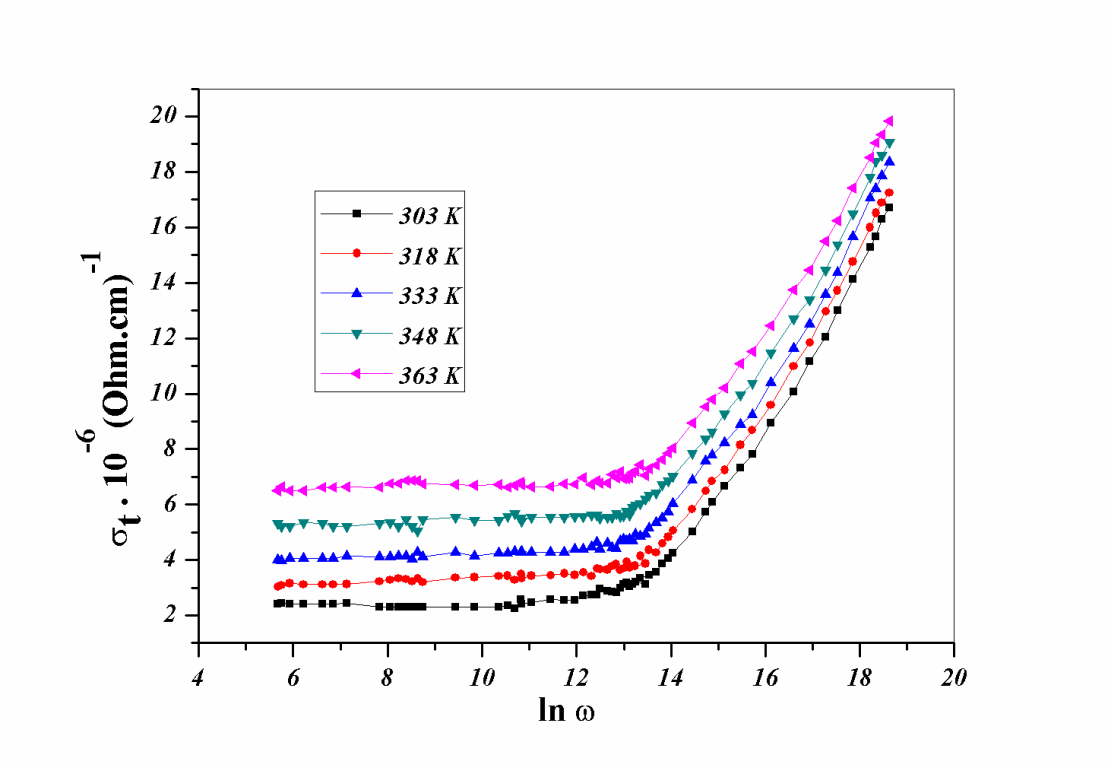

Fig 5. The total conductivity, $\sigma_t(\omega)$, as a function of frequency at various temperatures for DTNBI.

Figure 6 is illustrated the temperature dependence of dc electricalconductivity,σ_{dc} , of bulk DTNBI as noticed that σ_{dc} data fitted the Arhenius relation **[27-29]** where:

$$\sigma_{dc} = \sigma_0 \exp(-\Delta E_{dc} / k_B T) \quad (5)$$

where ΔE_{dc} is the thermal activation energy of dc conduction and$\sigma_0$is a pre-exponential parameter, which includes the density of states and the mobility of the charge carrier.A straight line for fitted values of σ_{dc} is seen in Fig.6 and from its slope, the thermal activation energy ΔE_{dc} is determined as 0.18 eV for bulk DTNBI.

The ac conductivity (σ_{ac}) of a material is described in terms of angular frequency ($\omega=2\pi f$) by the following relation [30]:

$$\sigma_{ac}(\omega) = A\omega^s \quad (6)$$

Here, the temperature-dependent constant is A. (s) knows as the frequency exponent, which depends on the temperature and used as an indication for the ac

conduction mechanism of the materials and get sufficient information on conducting system [25,31,32].

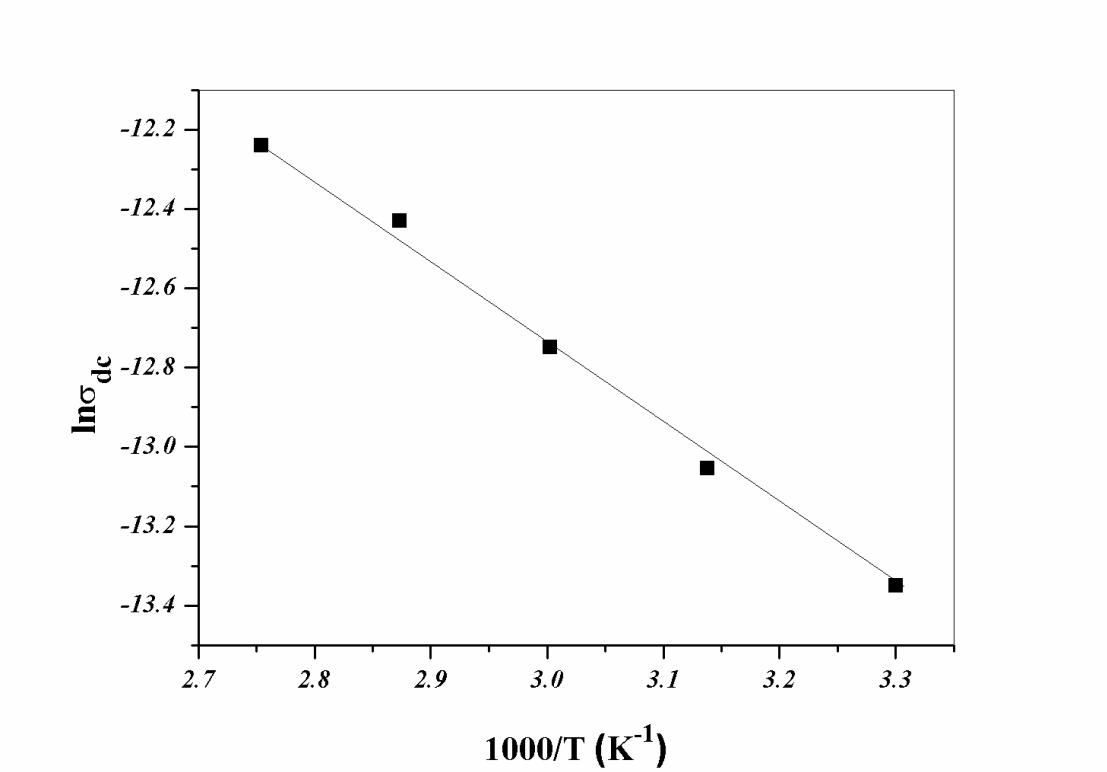

Fig 6. The temperature dependence of dc electrical conductivity of DTNBI.

The s values were estimated from the linear slope of [ln $\sigma_{ac}(\omega, T)$] versus [ln ω] as seen in Fig.7. At low range of frequency [40 Hz-30 kHz], s has a constant value equal to 0.09 ± 0.002. At high frequency, the value of the exponent frequency, s, was found as 0.6 at 303 K and decreased by small extent 0.5at 363 K for bulk DTNBI. The correlated barrier hopping (CBH) model helps to understand the obtained results of bulk DTNBI [33,34] and $\sigma_{ac}(\omega, T)$ conductivity according to this model is given by [35]:

$$\sigma_{ac}(\omega) = \frac{\pi^2[N(E_F)]^2\varepsilon}{24}\left(\frac{8e^2}{\varepsilon W_M}\right)^6 \frac{\omega^s}{\tau_o^{1-s}} \quad (7)$$

In the above equation;W_M is the maximum height of the potential barrier over which the electrons hop, $N(E_F)$ is the density of localized states, e is the electronic chargeand theτ_o is effective relaxation time.

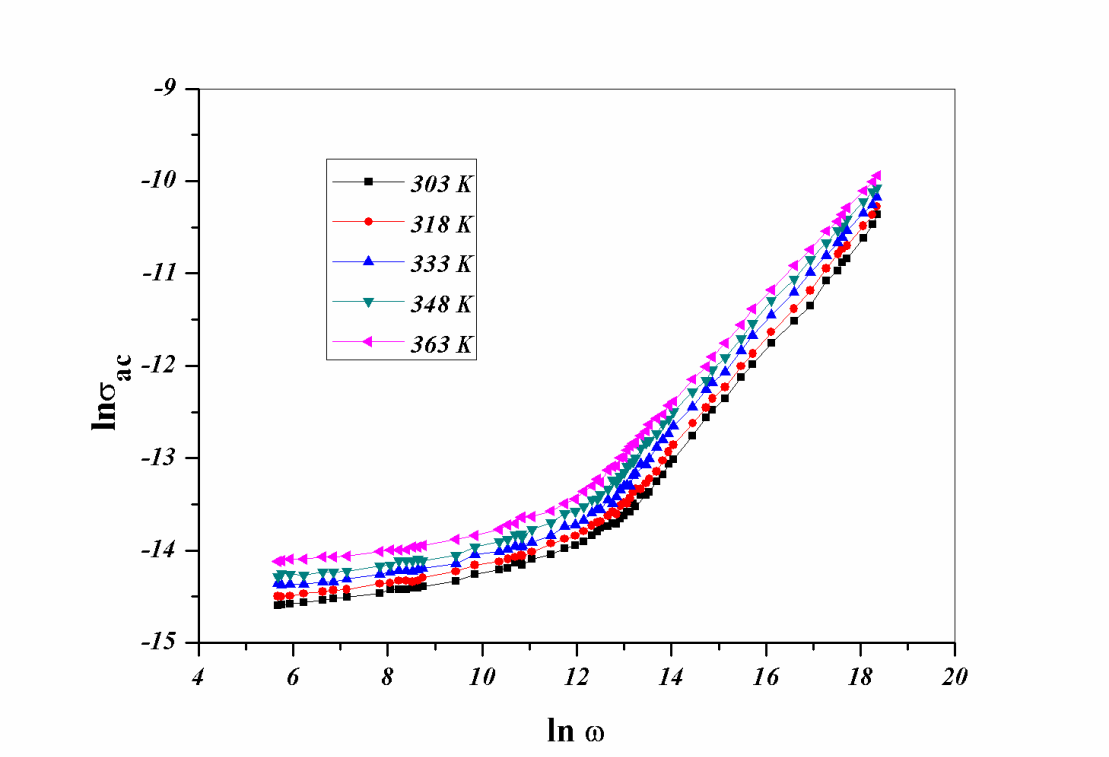

Fig 7. Frequency dependence of lnσ$_{ac}$ for DTNBI at different temperatures.

The ac conductivity ln $\sigma_{ac}(\omega)$ against(1000/T) is represented in Fig. 8 for bulk DTNBI at different frequencies. It is shown that from this figure $\sigma_{ac}(\omega)$ increased with the reciprocal of the temperature. The $\sigma_{ac}(\omega)$ has a thermal activation mechanism according to this dependence and it can be measured using the Arrhenius equation:

$$\sigma_{ac} = \sigma_u \exp(-\Delta E_{ac} / k_B T) \quad (8)$$

where σ_u is a constant, ΔE_{ac} is the activation energy under the ac fields. In Fig. 8, from the slopes of the obtained straight lines, the activation energy ΔE_{ac}, of ac conduction behavior was calculatedwith various frequencies. ΔE_{ac} was found as 0.098 eV at 30 kHz and decreased to 0.066 eV at 200 kHz by increasing frequency according to Table 2. The determined ΔE_{ac} value of ac conduction was noticed that it was lower than the dc conduction for bulk DTNBI. This result clarified that the carriers of charge in dc conduction take the easiest way including some large jumps, while in ac conduction this is not so important [36].

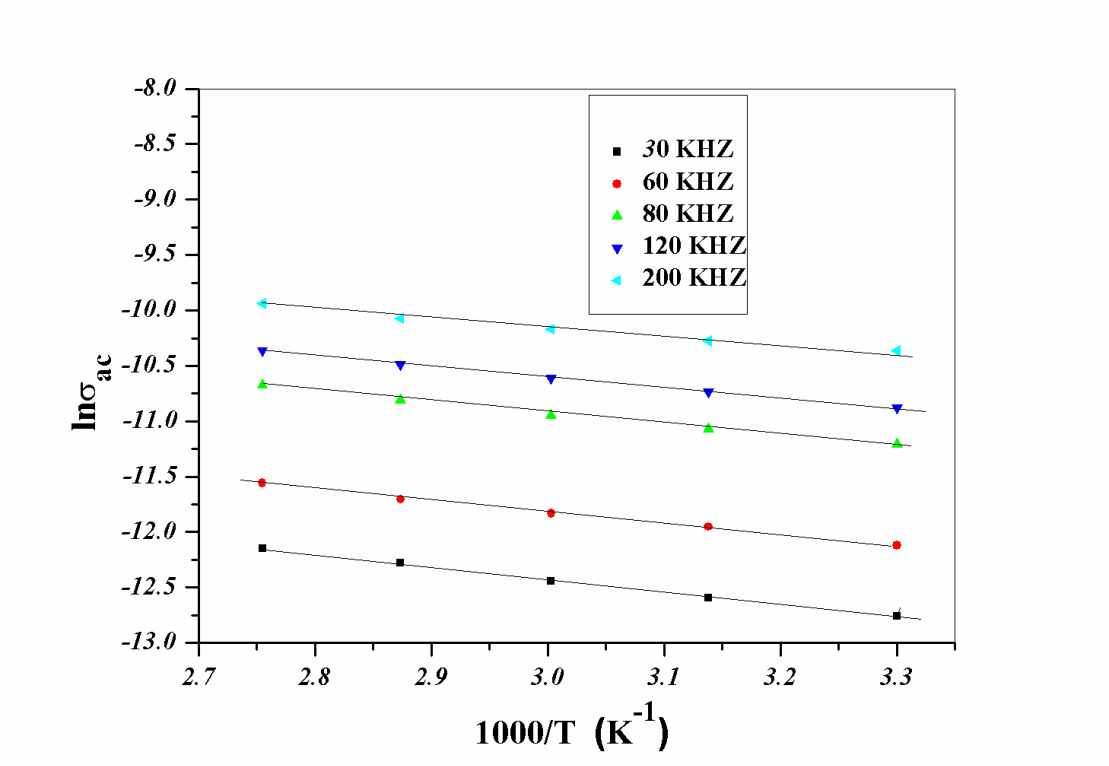

Fig 8. Temperature dependence of ac conductivity for DTNBI at different frequencies.

Table 2 : The activation energy of ac conduction ΔE_{ac} at different frequencies of DTNBI.

Frequency (kHz)	30	60	80	120	200
ΔE_{ac} (eV)	0.098	0.087	0.085	0.081	0.066

3.3 Dielectric Property Dependence :

Different forms of polarization (electronic, ionic, relaxation and space charge) are correlated with the dielectric properties of materials [37,38]. These forms of polarization offers an enhanced understanding of the electrical properties of the materials upon the variation of temperature and frequency, where a material's complex dielectric constant (ε^*) is given by [39]:

$$\varepsilon^* = \varepsilon_1 + i\,\varepsilon_2 \qquad (9)$$

where ε_1 is the real part of dielectric constant and it is a measure of the energy preserved in the material as aresult of the applied electric field and specifies the

strength of alignment of dipoles in the dielectric. ε_2 is the imaginary part of dielectric constant and it is being the energy dissipated in the dielectric.

In Figs. 9 and 10, the frequency dependence of ε_1 and ε_2 of bulk DTNBI at different temperatures are displayed. Fromthese figures,ε_1 and $\varepsilon_2$are decreasing with an increaseof the frequency used.This is reflected by the material's dielectric polarization mechanism, which takes the form of interfacial, ionic, or electronic dipolar polarization. In the high-frequency range, ionic and electronic polarizations are dominant, while interfacial dipolar polarization is dominant in the low range of frequency. Interfacial polarization caused by space charges created in the material induced image charges on the electrodes in the low-frequency range is responsible for the growth of both ε_1 and ε_2.Defects and a localized charge accumulation sculpted at the electrode and sample interface have captured these space charges are migrates under the electric field action [40-42].

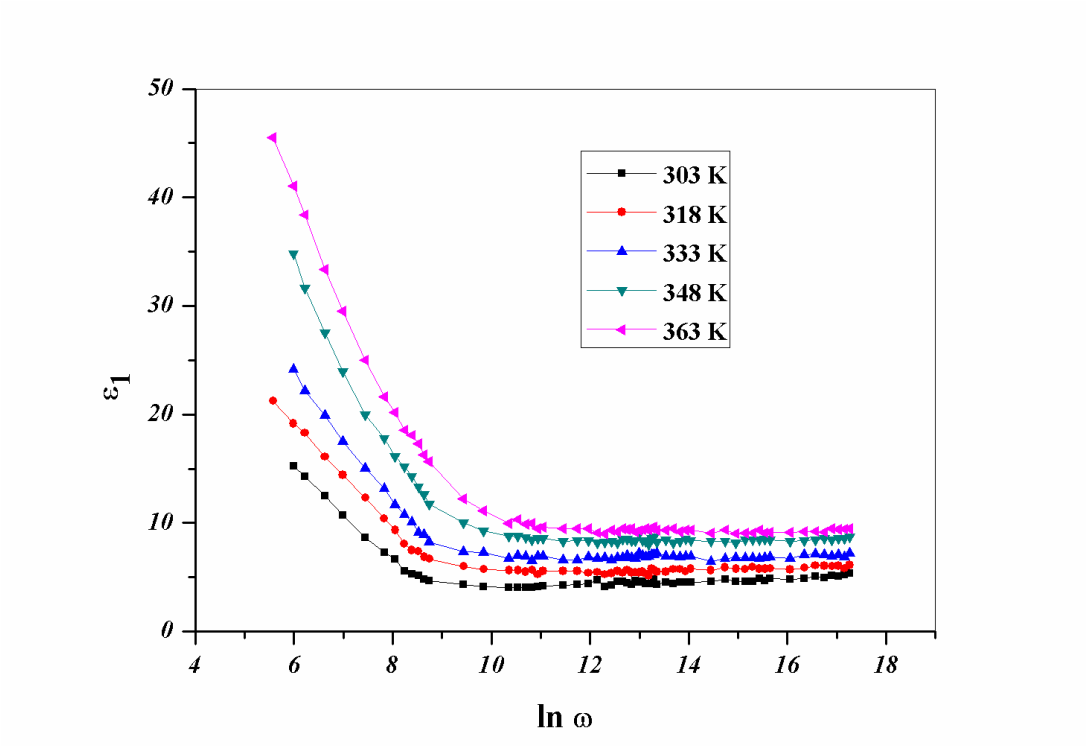

Fig 9. Frequency dependence of dielectric constant (ε_1) of DTNBI at different temperatures.

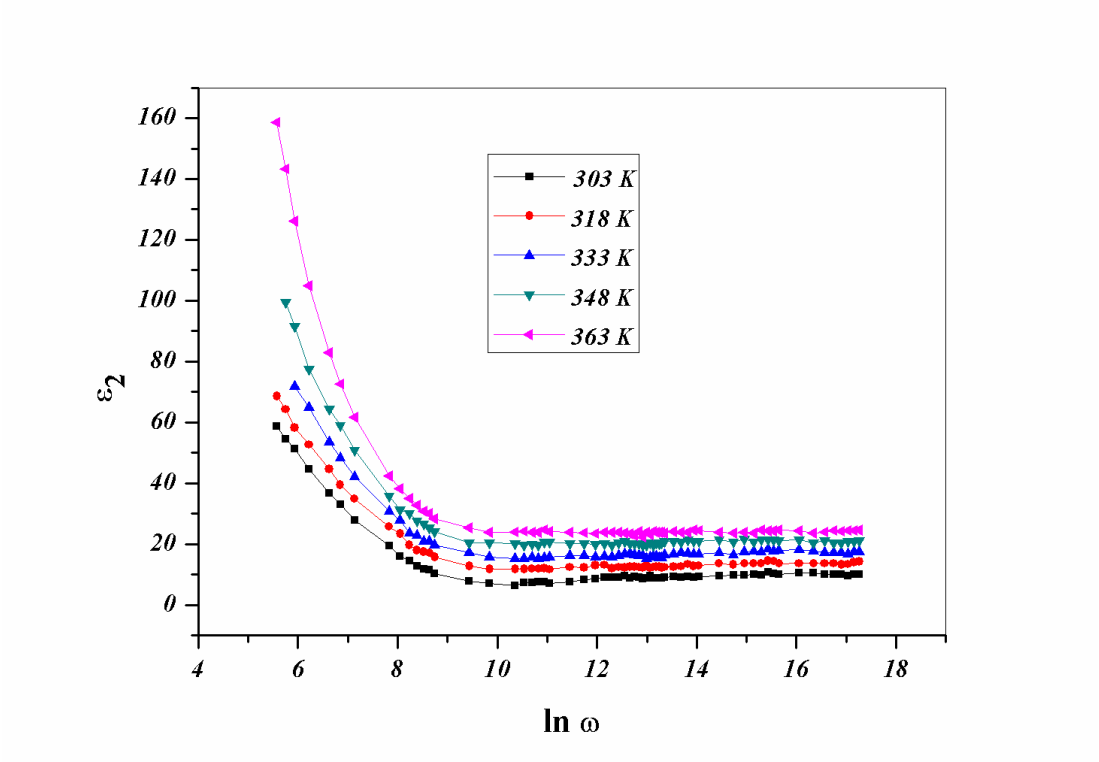

Fig 10. Frequency dependence of dielectric loss (ε_2) of DTNBI at different temperatures.

Figures 11 and 12 show the temperature dependence of both ε_1 and $\varepsilon_2$at different frequencies for bulk DTNBI. Dielectric constants $\varepsilon_1$and$\varepsilon_2$increased as the temperature increased over the whole range of frequencies tested, as seen in Figs.11 and 12. This could be because dipoles in polar materials cannot orient themselves at low temperatures, whereas dipole orientation is straightforward at higher temperatures, and therefore the orientation polarization value tends to grow, causing the temperature dielectric constant to rise.The influence of molecular interaction energy becomes smaller than the effect of thermal energy, resulting in an increase of ε_1 and ε_2 as temperature rises [43].

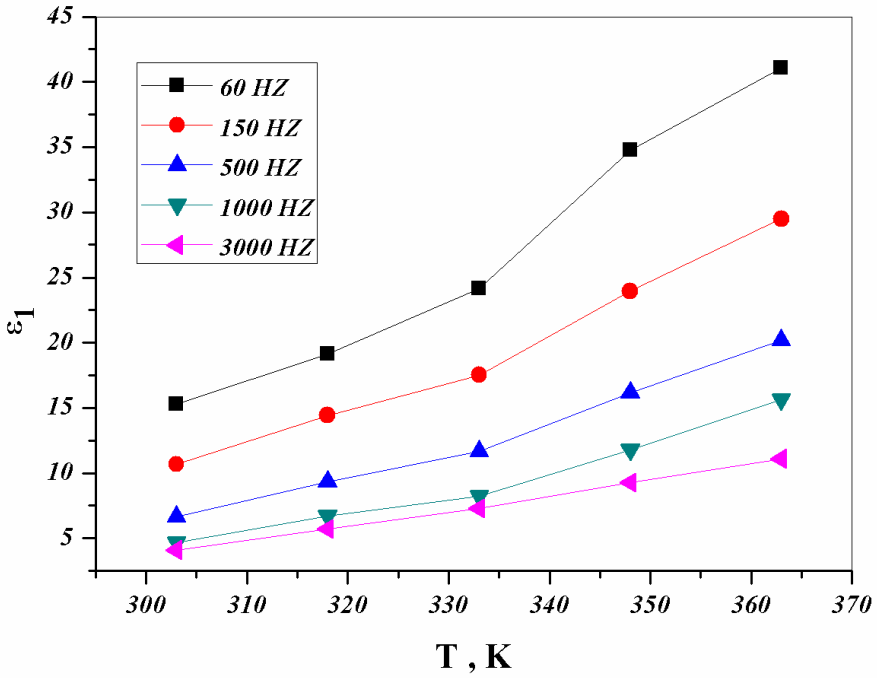

Fig 11. The temperature dependence of dielectric constant (ε_1) of DTNBI at different frequencies.

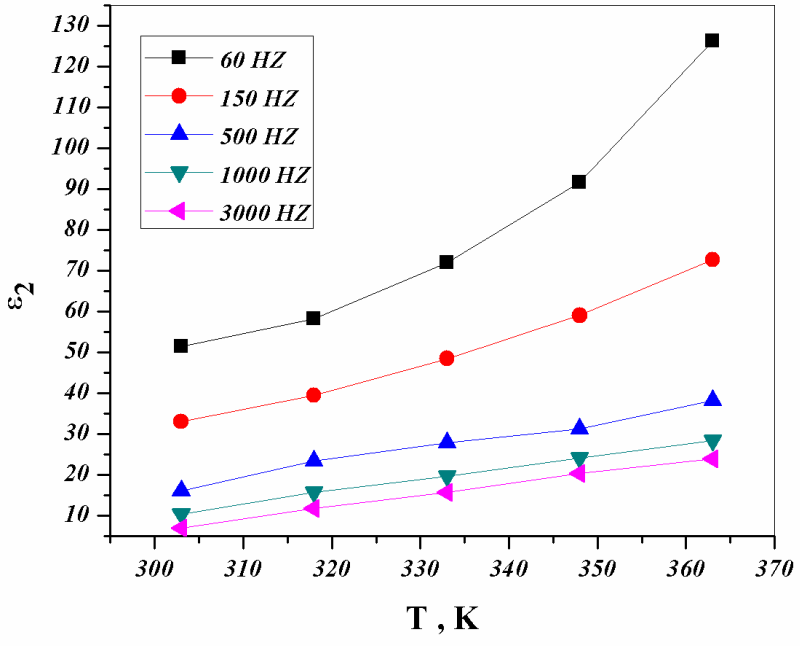

Fig 12. The temperature dependence of dielectric loss (ε_2) of DTNBI at different frequencies.

At a certain frequency, the imaginary part of complex dielectric constant ε_2 (in which dielectric dispersion exists) isexpressedby Guntini et al. [44] as:

$$\varepsilon_2 = B\ \omega^m \quad (10)$$

As seen in Fig.13, The slopes of ln ε_2 against lnω at various temperatures are used to calculate the power m of this equation. Figure 14 shows the alternation in m values as a function of temperature. The following equation correlates the exponent m to the temperature and maximum barrier height W_m:

$$m = -4k_BT/W_m \quad (11)$$

The change of m values against T is shown in Fig 14 and it is showed that m reduces withrising temperature. Value of $W_m$was determined to be equal to 0.15 eV.

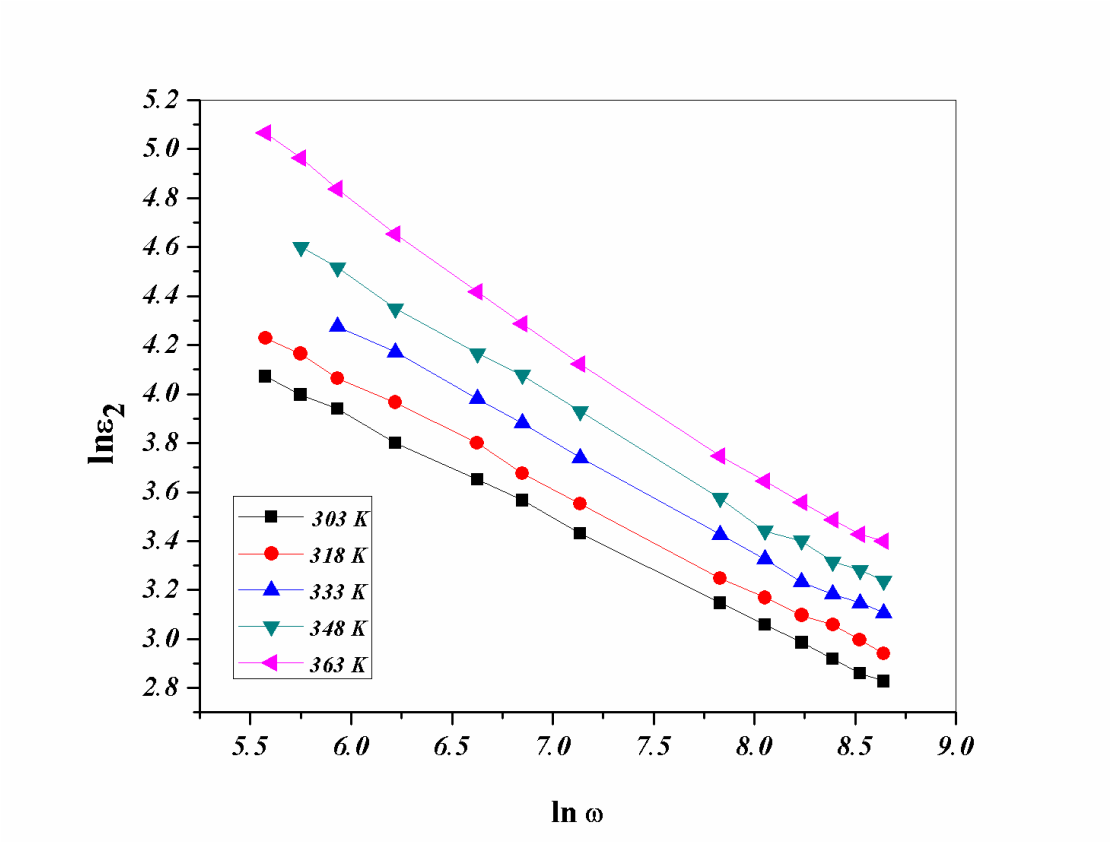

Fig 13. Variation of lnε$_2$ aganist lnω of DTNBI at different temperatures.

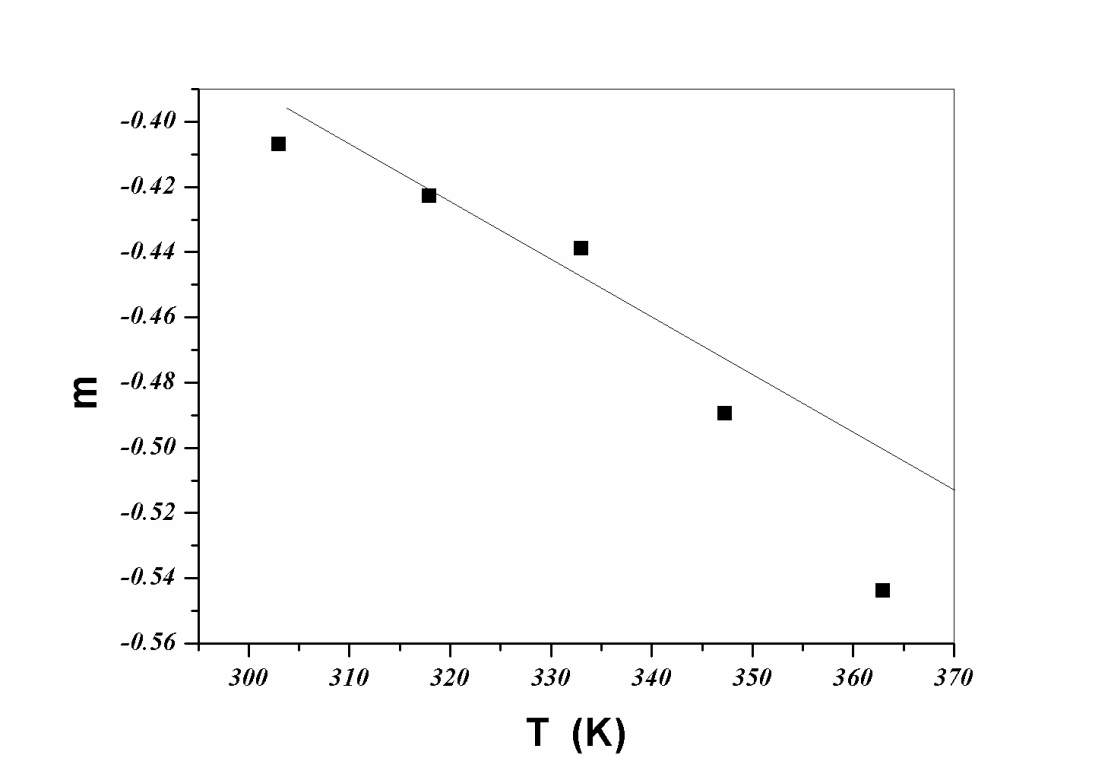

Fig 14. Temperature dependence for exponent m of DTNBI.

In addition, the complex electric modules $M^*(\omega)$ is generated using the complex permittivity equation [45] and the real and imaginary parts of M^*(M' and M'', respectively) are found from ε_1 and ε_2 values according to the Macedo et al. equation [46] as follows:

$$M^*(\omega) = 1/\varepsilon^*(\omega), M^*(\omega) = M' + iM'' \quad (12)$$

$$M'(\omega) = \varepsilon_1/[(\varepsilon_1)^2 + (\varepsilon_2)^2] \quad (13)$$

$$M''(\omega) = \varepsilon_2/[(\varepsilon_1)^2 + (\varepsilon_2)^2] \quad (14)$$

M' and M'' of bulk DTNBI are studied as a function of frequency at different temperatures, as illustrated in Figs. 15 and 16. The curves of M' in Fig. 15 show a markable change in M' with the change in the temperature, where at each frequency M' value decreased with rising temperature. It is noticed from that there is a low value of M' in the low frequency region which then it increases to a maximum value with increasing frequencyand it decreased at a higher value of frequency to reach a constant value. The tendency of saturation supports the suggestion that the short-range mobility of charge carriers is a mechanism of conduction[47].

The obtained modulus is depicted in Fig. 16 of bulk DTNBI, where values trend to zero in the low-frequency range, indicating that electrode effects have a minor impact and can thus be ignored [48]. The plots of this figure are described by the existence of the peak of relaxation. A simple indication of the real dielectric relaxation process is the occurrence of peaks in M′′. The frequency area below the highest peak defines the range where in charge carriers are mobiles on long-range distances.

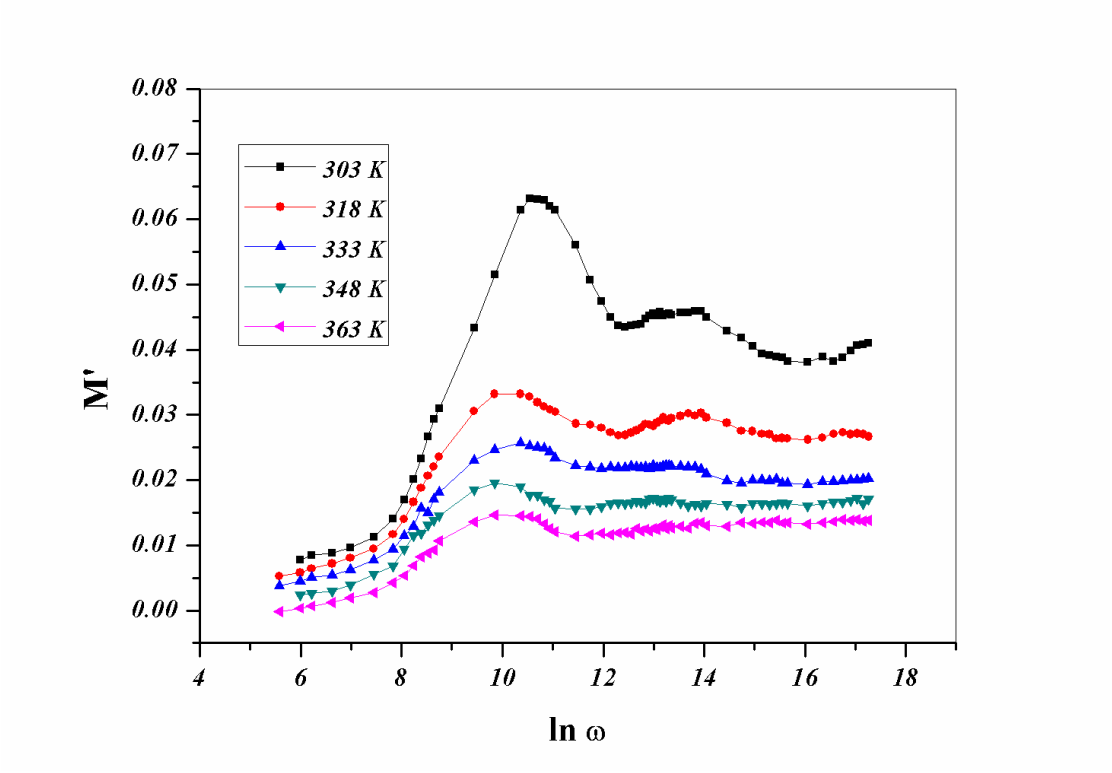

Fig 15. Frequency dependence of real part of complex electric modulus M′ of DTNBI at different temperatures.

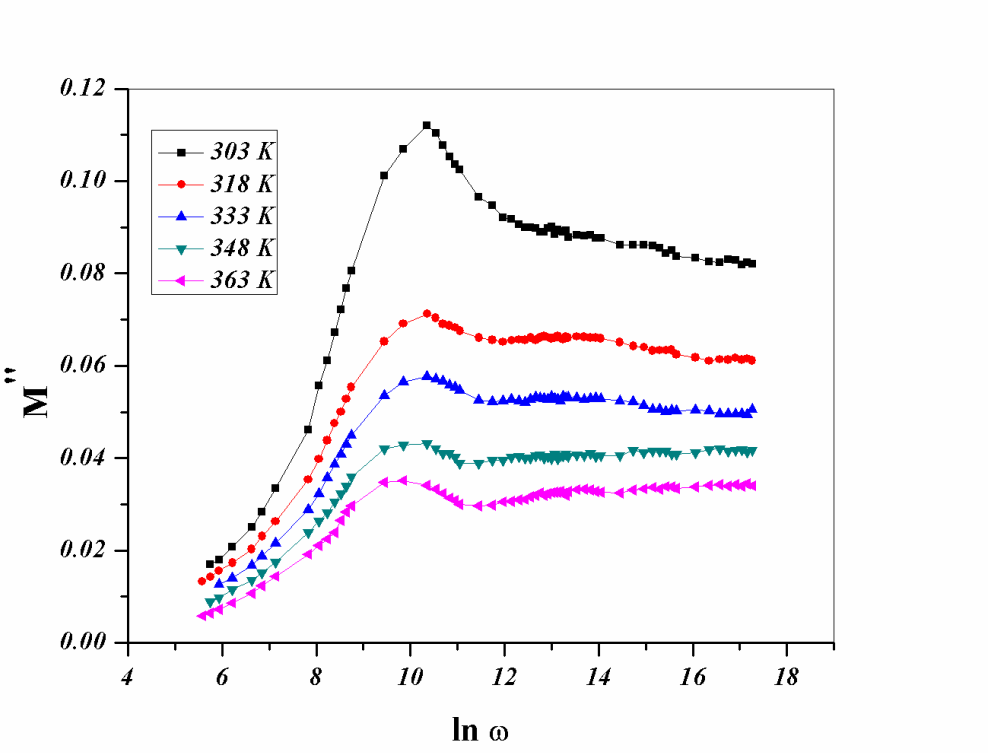

Fig 16. Frequency dependence of imaginary part of complex electric modulus M″ of DTNBI at different temperatures.

4. Conclusion

The structural properties of 1',3'-dihydro-1',3',3'-trimethyl-6-nitrospiro[2H-1-benzopyran-2,2'-[2H]indole], DTNBI, were examined by using XRD technique. the powder of DTNBI has a polycrystalline monoclinic structure. The resulted lattice constants were a = 29.912 Å, b = 18.815 Å, and c = 13.062 Å. The average crystallite size was 29.75 nm, according to Scherrer's equation. As well as this, according to the Williamson – Hall and Size-Strain plot methodologies, it was calculated to be 36.6 and 22.9 nm, respectively. Using both procedures, the determined strain has comparable values.The temperature dependence of DC and AC conductivity of bulk DTNBI presented by Arrhenius behavior with activation energies ΔE_{dc}as 0.18 eV and $\Delta E_{ac}$was≈ 0.098 eV at 30 kHz and decreased by growing frequency to 0.066 eV at 200 kHz. When the ac conductivity and its frequency exponent were analyzed, it was discovered that s has a constant value of 0.092 at low frequencies and s< 1 at high frequencies, s decreased as the temperature increased. The prevailing mechanism for the ac conduction was the model of correlated barrier hopping. The dielectric polarization mechanism of bulk DTNBI can explain the behavior of the real, ε_1, and

imaginary, ε_2, components of the complex dielectric constant depend on the temperature and frequency. The maximum barrier height W_m,of bulk DTNBI was calculated to be 0.15 eV according to Guntini's equation.At each frequency, the M′ value decreases with increasing temperature and the occurrence of peaks in M′′ indicates that the dielectric relaxation process is taking place.

5. References:

[1] A. Tomkeviciene, J.V. Grazulevicius, Glass-forming organic semiconductors for optoelectronics, Mater. Sci. 17: (2011) 335-342.

[2] Sh.A.Mansour, I.S.Yahia,G.B.Sakr, Electrical conductivity and dielectric relaxation behavior of fluorescein sodium salt (FSS)**,** SolidState Communications 150: (2010) 1386–1391.

[3] N.A. Azarova, J.W. Owen, C.A. McLellan, M.A. Grimminger, E.K. Chapman, J.E. Anthony, O.D. Jurchescu, Fabrication of organic thin-film transistors by spray-deposition for low-cost, large-area electronics, Org. Electron. 11: (2010) 1960-1965.

[4] B. Li, J. Chen, Y. Zhao, D. Yang, D. Ma, Effects of carrier trapping and scattering on hole transport properties of *N*,*N*′-diphenyl-*N*,*N*′-bis(1-naphthyl)-1,1′-biphenyl-4,4′-diamine thin films, Org. Electron. 12: (2011) 974-979.

[5] D. Manoharan, J. Chandrasekaran, S. Maruthamuthu, P. Jayamurugan, Poly(aniline-co-*o*-toluidine):poly(styrene sulfonic acid) nanocolloidal self assembled multilayer thin films as a hole transport layer in organic solar cells, Materials Science in Semiconductor Processing 34: (2015) 382–389.

[6] L. El Chaar, L.A. lamont, N.El Zein, Review of photovoltaic technologies, Renew. Sustainable Energy Rev. 15: (2011) 2165-2175.

[7] A. R. Murad, A. Iraqi, S. B. Aziz, S. N. Abdullah, M. A. Brza, Conducting Polymers for Optoelectronic Devices and Organic Solar Cells: A Review, Polymers 12: (2020) 2627-2674.

[8] S. Ojha, M. Roy, A.Chamuah, K. Bhattacharya, S. Bhattacharya, AC conductivity and dielectric behavior of Cu-S-Te chalcogenide glassy system, Materials Letters 258: (2020) 126792-4.

[9] A. Kr. Bar, K. Bhattacharya, R. Kundu, D. Roy, S. Bhattacharya, Electrical relaxation and grain boundary effect in CdI_2 doped glass-nanocomposites, Journal of Non-Crystalline Solids 452: (2016) 169–175.

[10] A. Kr. Bar, D. Roy, S. Bhattacharya, Relaxation of Cu^{+2} Ions in Molybdate Glass-Nanocomposites, Advanced Science Focus, 2 : (2014) 155-158.

[11] S. Bhattacharya, D. Roy , M. P. F. Graca, M. A. Valente , A.Kr. Bar, Dielectric Behavior of Iodomolybdate Glass-Nanocomposites , Advanced Science Letters, 3 : (2010) 523-526.

[12] M.V. Alfimov, O.A. Fedorova, Gromov SP, Photoswitchable molecular receptors, J PhotochemPhotobiol A-Chem 158: (2003) 183-198.

[13] J.Zhang, Jing.Li, Mengmeng.Huo, Naixu.Li, Jiancheng.Z, Tuoqi.Li, JingJiang. Photochromic Inorganic/Organic ThermoplasticElastomers, Macromolecular Rapid Communications**,** *38 (2017*) 1700210-1700219.

[14] R.Klajn, Spiropyran-based dynamic materials, Chem. Soc. Rev., 43**:** (2014) 148-184.

[15] A.A.Ali, R Kharbash, Y. Kim, Chemo- and biosensing applications of spiropyran and its derivatives - A review, Analytica Chimica Acta 1110 : (2020) 199 – 223.

[16] E.N-Borhani, A. Abdollahi, H.Roghani-Mamaqani,M.Salami-Kalajahi, Photoswitchable surface wettability of ultrahydrophobic nanofibrous coatings composed of spiropyran-acrylic copolymers, Journal of Colloid and Interface Science 593 : (2021) 67–78.

[17] M. M. El-Nahass, W. M. Desoky, Investigating the structural and optical properties of thermally evaporated 1,3,3-trimethylindolino-β-naphthopyrylospiran thin films, Appl. Phys. A, 123: (2017) 517-525.

[18] I.S. Elashmawi, E.M. Abdelrazek, A.M. Hezma, A. Raje, Modification and development of electrical and magnetic properties of PVA/PEO incorporated with $MnCl_2$, Physica B 434: (2014) 57–63.

[19] W.M. Desoky, Structural, AC conductivity and dielectric properties of bulk 1,3-Dihydro-1,3,3-trimethylspiro[2H-indole-2,3′-[3H]naphth[2,1-b][1,4]oxazine], Arab J. Nucl. Sci. Appl., 52: (2019) 196-203**.**

[20] Eman. K Tawfik, Wael H.Eisa, N. Okasha, H.A.ashry, Influence of annealing temperature of α- Fe2O3 nanoparticles on Structure and Optical Properties, J. Sci. Res. Sci., 37: (2020) 73-91.

[21] R.Kundua, D. Roy, S. Bhattacharya, Microstructure, electrical conductivity and modulus spectra of CdI_2 doped nanocomposite-electrolytes, Physica B 507: (2017) 107–113.

[22] S. Ojha, M.Roy, A.Chamuah, K. Bhattacharya, S. Bhattacharya, Transport phenomena of Cu–S–Te chalcogenide nanocomposites: frequency response and AC conductivity, Phys. Chem. Chem. Phys., 22: (2020) 24600-24613.

[23] D. Nath, F. Singh, R. Das, X-ray diffraction analysis by Williamson-Hall, Halder-Wagner and size-strain plot methods of CdSe nanoparticles- a comparative study, Materials Chemistry and Physics 239: (2020) 122021-122030.

[24] M. khan, A. Mishra, J. Shukla, P. Sharma, X-ray analysis of $BaTiO_3$ ceramics by Williamson-Hall and size strain plot methods, AIP Conference Proceedings 2100: (2019) 020138-020142.

[25] A. Kr Bar, K. Bhattacharya, R. Kundu, D. Roy, S. Bhattacharya, Anomalous electrical conductivity in selenite glassy nanocomposites Materials Chemistry and Physics 199: (2017) 322-328.

[26] E. F. M. El-Zaidia, E. A. El-Shazly, H. A. M. Ali, Estimation of Electrical Conductivity and Impedance Spectroscopic of Bulk $CdIn_2Se_4$ Chalcogenide Journal of Inorganic and Organometallic Polymers and Materials 30: (2020) 2979-2986.

[27] S.S.Chaid, Annealing Temperature Effects on the Optical Properties of CdO Thin Films Deposited by CSP TechniqueInternational Letters of Chemistry, Physics and Astronomy, 42: (2015) 63- 71.

[28] F. Ben Bacha, KGuidara, M. Dammak, M. Megdiche, AC and DC conductivity study of ceramic compound $NaGd(WO_4)_2$ using impedance spectroscopy, J Mater Sci: Mater Electron, 28: (2017) 10630–10639.

[29] G.Nava , F. Fumagalli , S. Gambino , I. Farella , G. Dell'Erba, D. Beretta , G. Divitini, C. Ducati , M. Caironi , A. Cola, F.Di. Fonzo, owards an electronic grade nanoparticle-assembled silicon thin film by ballistic deposition at room temperature: the deposition method, and structural and electronic properties, J. Mater. Chem. C, 5:(2017) 3725-3735.

[30] B. Louati, M Gargouri, K Guidara, T Mhiri, AC electrical properties of the mixed crystal $(NH_4)_3H(SO_4)_{1.42}(SeO_4)_{0.58,}$ Journal of Physics and Chemistry of Solids 66: (2005) 762–765**.**

[31] R.Kunduab, D. Roy, S. Bhattacharya, Electrical Transport of Mixed Phased Glassy Nanocomposites, Transactions of the Indian Ceramic Society, 74: (2015) 35-40.

[32] S. Bhattacharya and A. Ghosh, Conductivity spectra in fast ion conducting glasses: Mobile ions contributing to transport process, Phys. Rev. B 70 : (2004) 172203 – 4.

[33] M. E. Sayed, M. M. Elokr , L. I. Soliman, H. A. Zayed, Synthesis and characterization of Li2O modified sodium phosphate glasses, J. Sci. Res. Sci.35: (2018) 417-438.

[34] S.R. Elliott, A theory of a.c. conduction in chalcogenide glasses, Philos. Mag. 36: (1977) 1291- 1304.

[35] M.M. El-Nahass, H.A.M. Ali, AC conductivity and dielectric behavior of bulk Furfurylidenemalononitrile, Solid State Communications 152: (2012) 1084–1088.

[36] SR. Lukić-Petrović, F. Skuban, DM. Petrović, M. Slankamenac, Effect of copper on DC and AC conductivities of (As_2Se_3)–(AsI_3) glassy semiconductors, Journal of Non-Crystalline Solids 356: (2010) 2409-2413.

[37] K.C. Kao, H,book of Dielectric Phenomena in Solids, Elsevier ,(2004) Academic Press.

[38] C.A. Harper, H, book of Ceramics, Glasses, Diamond, McGraw Hill, (2001) New York.

[39] M.M. El-Nahass, H.A.M. Ali, AC conductivity and dielectric behavior of bulk Furfurylidenemalononitrile, Solid State Commun. 152: (2012) 1084-1088.

[40] S. Kurien, J. Mathew, S. Sebastian, S.N. Potty, Kc. George, Dielectric behavior and ac electrical conductivity of nanocrystalline nickel aluminate, Mater Chem. Phys. 98: (2006) 470 - 476.

[41] N. Kumar, S. Chand, Efects of temperature, bias and frequency on the dielectric properties and electrical conductivity of Ni/SiO2/p-Si/ Al MIS Schottky diodes, Journal of Alloys and Compounds 817: (2020) 153294-6.

[42] P.S. Anantha, K. Harihanan, ac Conductivity analysis and dielectric relaxation behaviour of $NaNO_3$–Al_2O_3 composites, Mater. Sci. Eng. B 121: (2005) 12 - 19.

[43] N.S hukla, V. Kumar , D. K. Dwlvedi, DEPENDENCE OF DIELECTRIC PARAMETERS AND A.C. CONDUCTIVITY ON FREQUENCY AND TEMPERATURE IN BULK Se90Cd8In2 GLASSY ALLOY, Journal of Non-Oxide Glasses 8 : (2016) 47 – 57.

[44] N. F. Osman , M. M. Elokr , L. I. Soliman , H. A. Zayed, Synthesis and study of electrical properties of Li2O modified P2O5-ZnO-Na2O glasses, J. Sci. Res. Sci., 36: (2019) 163-168.

[45] B.G. Soares, M.E. Leyva, G.M.O. Barra, D. Khastgir, Dielectric behavior of polyaniline synthesized by different techniques, Eur.Polym. J. 42: (2006) 676 - 686.

[46] P.B. Macedo, C.T. Moynihan, R. Bose, THE ROLE OF IONIC DIFFUSION IN POLARISATION IN VITREOUS IONIC CONDUCTORS, Phys. Chem. Glasses. 13 :(1972) 171-179.

[47] M. BelblHossen, A. K. M. Akther Hossain, omplex impedance and electric modulus studies of magnetic ceramic $Ni_{0.27}Cu_{0.10}Zn_{0.63}Fe_2O_4$, Journal of Advanced Ceramics, 4 : (2015)217- 225.

[48] G. M Tsangaris, G. C Psarras ,N Kouloumbi , Electric modulus and interfacial polarization in composite polymeric systems, Journal ofMaterials Science , 33 : (1998)2027–2037 .

الملخص العربى

دراسه الخصائص التركيبيه والتوصيليه الكهربيه وثابت العزل للمركب

1',3'-dihydro-1',3',3'-trimethyl-6-nitrospiro[2H-1-benzopyran-2,2'-[2H]indole]

ايمان عماد الدين محمود[1]- محمود محمد النحاس[2] – حمديه عبد الحميد زايد[1] – هند محمد على[2]

1- قسم الفيزياء – كلية البنات الأداب والعلوم والتربية – جامعة عين شمس – القاهرة – جمهورية مصر العربية.

2- قسم الفيزياء – كلية التربية – جامعة عين شمس ص ب 11757 القاهرة – جمهورية مصر العربية.

يتناول البحث دراسة الخصائص التركيبية للمركب

1',3'-dihydro-1',3',3'-trimethyl-6-nitrospiro[2H-1-benzopyran-2,2'-[2H]indole]

والذي يرمز له بالاختصار DTNBI.وقد تم دراسة تركيب المركب في صورته كمسحوق باستخدام تقنية حيود الاشعة السينية XRD حيث أظهرت النتائج ان التركيب البلوري للمركب DTNBI يكون عديد التبلور ينتمي إلي النظام احادي الميل . كما تم تعيين متوسط حجم البلورات باستخدام كلا من طرق Scherrer's formula و Williamson-Hall و Size-Strain plots. كما تم قياس الموصلية الكهربية بالتيار المتردد وخصائص العزل الكهربي للمركب DTNBI المضغوط على هيئة اقراص في نطاق الترددات من 40 هرتزإلى 5 ميجاهرتز وفي مدى درجة الحرارة 303-363 كلفن. وقد أوضح البحث ايضا أن الموصلية الكهربية للتيار المتردد والتيار المستمر تتبع قانون Arrhenius . كما تم تحديد طاقة التنشيط للموصلية الكهربية بالتيارالمتردد وتم تحليل خصائص العزل باستخدام طريقة electric modulus formalism.